Rheological and Light Scattering Studies of Cationic Fluorocarbon Surfactant Solutions at Low Ionic Strength

ARTICLE *in* LANGMUIR · MARCH 2002

Impact Factor: 4.46 · DOI: 10.1021/la015687v

5 AUTHORS, INCLUDING:

Eric Buhler
Paris Diderot University
61 PUBLICATIONS **1,349** CITATIONS
SEE PROFILE

Candau Sauveur
University of Strasbourg
137 PUBLICATIONS **6,660** CITATIONS
SEE PROFILE

Rheological and Light Scattering Studies of Cationic Fluorocarbon Surfactant Solutions at Low Ionic Strength

Cl. Oelschlaeger,[†] G. Waton,[†] E. Buhler,[‡] S. J. Candau,*[,†] and M. E. Cates[§]

Laboratoire de Dynamique des Fluides Complexes, UMR No. 7506, C.N.R.S. - U.L.P., 4 rue Blaise Pascal, 67070 Strasbourg Cedex, France, Centre de Recherches sur les Macromolécules Végétales-CNRS, affiliated with Joseph Fourier University, BP53, 38041 Grenoble, Cedex 9, France, and The University of Edinburgh, James Clerk Maxwell Building, Department of Physics and Astronomy, The King's Buildings, Mayfield Road, Edinburgh EH9 3JZ, United Kingdom

Received November 19, 2001. In Final Form: January 18, 2002

The structural and dynamic properties of low ionic strength micellar solutions of the cationic surfactant perfluorooctylbutane trimethylammonium bromide have been investigated by means of dynamic and static light scattering and rheological experiments. In the range of concentration extending from the critical micelle concentration to about the overlap concentration, the surfactant self-assembles into micellar aggregates with sizes of the order of 100 nm. At higher concentrations, the system is characterized by a single correlation length consistent with the formation of a transient network of wormlike micelles. In the dilute regime, the solutions exhibit a very large shear thickening effect (up to 50) and a very slow recovery (hours) after a thermal or mechanical perturbation. The extent of consistency of the dynamical observations with the various possible structures inferred from the scattering data has been discussed. Some arguments are in favor of the presence of interlinked micellar rings in the quiescent state, which was suggested in a recent theoretical model.

Introduction

Under appropriate conditions, surfactants in solutions self-assemble to form long cylindrical micelles. In the dilute regime, that is, at volume fractions below the overlap threshold C^*, the solutions often exhibit under shear complex time-dependent and history-dependent flow behaviors.[1−16] A most puzzling effect, first studied by Hoffmann and co-workers, is the dramatic shear thickening observed above a critical shear rate for many systems, primarily ionic surfactants at low ionic strength. The increase in stress associated with the shear thickening occurs after a latency time following the onset of steady shear. Then, the stress evolves slowly over very long periods of times (up to hours) before achieving steady state. A similarly slow time scale controls the disappearance of structural memory after the shear has been terminated as revealed by rheological[15] and scattering[17,18] experiments performed after a rheological disturbance.

Furthermore, it was shown recently that the transient mechanical response depends drastically on the thermal history of the sample.[15]

On the theoretical side, shear thickening has been attributed to shear-induced alignment causing end-to-end fusion of small rodlike micelles, leading to the formation of a network of long micelles.[6,19,20] The presence of monodisperse particles small enough not to overlap at $C < C^*$ was commonly accepted on the basis of theoretical predictions[21] and of small-angle neutron scattering (SANS) results, compatible with rod lengths of several tens of nanometers.[12,14,22,23] In the above model, the shear-induced gelation occurs when the shear rate becomes comparable to the rotational diffusion constant of the micellar rods in the quiescent system. In fact, as pointed out by several authors, the measured critical shear rates $\dot{\gamma}_c$ are several orders of magnitude lower than the rotational diffusion rates calculated for rods with sizes of a few tens of nanometers.[6,9,14]

[†] Laboratoire de Dynamique des Fluides Complexes.
[‡] Centre de Recherches sur les Macromolécules Végétales-CNRS.
[§] The University of Edinburgh.

(1) Hoffmann, H.; Platz, G.; Rehage, H.; Schorr, W.; Ulbricht, W. *Ber. Bunsen-Ges. Phys. Chem.* **1981**, *85*, 255−266.
(2) Rehage, H.; Hoffmann, H. *Rheol. Acta* **1982**, *21*, 561−563.
(3) Hoffmann, H.; Löbl, M.; Rehage, H.; Wunderlich, I. *Tenside Deterg.* **1985**, *22*, 290.
(4) Ohlendorf, D.; Interthal, W.; Hoffmann, H. *Rheol. Acta* **1986**, *25*, 468.
(5) Wunderlich, I.; Hoffmann, H.; Rehage, H. *Rheol. Acta* **1987**, *26*, 532.
(6) Hofmann, S.; Rauscher, A.; Hoffmann, H. *Ber. Bunsen-Ges. Phys. Chem.* **1991**, *95*, 2.
(7) Berwersdorff, H.-W.; Frings, B.; Lindner, P.; Oberthür, R. C. *Rheol. Acta* **1986**, *25*.
(8) Lindner, P.; Bewersdorff, H.-W.; Heen, R.; Sittart, P.; Thiel, H.; Langowski, J.; Oberthür, R. C. *Prog. Colloid Polym. Sci.* **1990**, *81*, 107−112.
(9) Oda, R.; Panizza, P.; Schmutz, M.; Lequeux, F. *Langmuir* **1997**, *13*, 6407−6412.
(10) Liu, C. H.; Pine, D. J. *Phys. Rev. Lett.* **1996**, *77*, 2121−2124.
(11) Boltenhagen, P.; Hu, Y.; Matthys, E. F.; Pine, D. J. *Phys. Rev. Lett.* **1997**, *79*, 2359−2362.
(12) Berret, J.-F.; Gamez-Corrales, R.; Oberdisse, J.; Walker, L. M.; Lindner, P. *Europhys. Lett.* **1998**, *41*, 677−682.
(13) Keller, S. L.; Boltenhagen, P.; Pine, D. J.; Zasadzinski, J. A. *Phys. Rev. Lett.* **1998**, *80*, 2725−2728.
(14) Gamez-Corrales, R.; Berret, J.-F.; Walker, L. M.; Oberdisse, J. *Langmuir* **1999**, *15*, 6755.
(15) Berret, J.-F.; Gamez-Corrales, R.; Lerouge, S.; Decruppe, J.-P. *Eur. Phys. J. E2* **2000**, 343.
(16) Hu, Y. T.; Matthys, E. F. *J. Rheol.* **1997**, *41*, 151.
(17) Oda, R.; Weber, V.; Lindner, P.; Pine, D. J.; Mendes, E.; Schosseler, F. *Langmuir* **2000**, *16*, 4859.
(18) Bellour, M.; Knaebel, A.; Munch, J. P.; Candau, S. J. *Eur. Phys. J. E3* **2000**, 343.
(19) Cates, M. E.; Turner, M. S. *Europhys. Lett.* **1990**, *7*, 681.
(20) Wang, S. Q.; Gelbart, W.; Ben-Shaul, A. *J. Phys. Chem.* **1990**, *94*, 2219.
(21) Mackintosh, F.; Safran, S.; Pincus, P. *Europhys. Lett.* **1990**, *12*, 697.
(22) Hoffmann, H.; Hofmann, S.; Rauscher, A.; Kalus, J. *Prog. Colloid Polym.* **1991**, *24*.
(23) Schmitt, V.; Schosseler, F.; Lequeux, F. *Europhys. Lett.* **1995**, *30*, 31.

10.1021/la015687v CCC: $22.00
Published on Web 00/00/0000 PAGE EST: 9.8

Recently, two new mechanisms for the formation of shear-induced structures were proposed. The first one assumes that electrostatic correlation-attractions lead to the formation of metastable bundles.[24] Under shear flow at shear rates $\dot{\gamma}$ larger than the unbinding time of micelles, the bundles form and grow in thickness. For solutions of sufficiently high concentration that are still unentangled, the micelles should aggregate into a network of bundles.

The second mechanism proposed is a ring-driven scenario.[25] The presence of micellar rings at $C < C^*$ is expected theoretically in the limit of high end-cap energy $E/2$ for the micelles. According to the model, the linking and delinking kinetics of large rings controls the shear-thickening process. Equilibrium between rings and open chains in turn controls the slow relaxations.

Both of these two mechanisms require the presence in the quiescent solutions at $C < C^*$ of large particles (bundles or large rings). Such large entities were not detected in the scarce light scattering[18,26] and the numerous SANS studies performed in salt-free micellar solutions.[12,14,22,23]

In this paper, we report on a study by light scattering and rheology of micellar solutions at low ionic strength of a fluorinated surfactant, at concentrations ranging from the critical micelle concentration (cmc) to above the overlap concentration. A distinctive property of the fluorocarbon surfactants is their tendency to form structures with relatively little curvature, such as cylindrical micelles and bilayer structures.[27,28] This is due to a higher hydrophobicity and higher stiffness of the fluorocarbon chains as compared to hydrocarbon homologues. Furthermore, the fluorocarbon tail cross-sectional area a_{tail} was estimated to be 31.5 Å^2 compared to 21.4 Å^2 for the hydrocarbon, resulting in a larger packing parameter a_{tail}/a_0, where a_0 is the effective polar headgroup area.[27] This would also favor the cylindrical curvature. One expects therefore for such surfactants a very large end-cap energy and the formation of very long cylindrical micelles or of rings at very low concentrations.

Another relevant observation is the quite large shear thickening reported for fluorocarbon surfactant solutions at concentrations close to the cmc,[3,29] compared to hydrocarbon homologues.

The dynamic and static light scattering experiments reported in this paper are aimed at elucidating the actual structure of the aggregates formed at concentrations between cmc and C^* both in salt-free solutions and in solutions containing small amounts of salt. The chosen salt was NaF as F^- which stands at one end of the Hofmeister series[30] does not likely bind to the cationic surfactant and its effect is only a screening of the electrostatic interactions.

The second aspect of the study concerns the rheological properties. The aim was to try to establish a possible correlation between the structure of the surfactant self-assemblies and the characteristics of the nonlinear effects and of the slow relaxation processes. Both light scattering and rheological properties showed an unexpected behavior. The presence of large micellar aggregates was found in the concentration range extending from the cmc and the overlap concentration. In the same concentration range, the solutions exhibit a marked shear thickening and a very slow structural recovery after a shear or thermal perturbation. The consistency of the dynamical properties with the various possible structures of the aggregates is discussed, and the experimental results are compared to the predictions of recent theoretical models.[24,25]

Materials and Methods

The perfluorooctylbutane trimethylammonium bromide [$C_8F_{17}(CH_2)_4N^+(CH_3)_3Br^-$ (M = 614 g/mol)] surfactant (C_8F_{17}) has been synthesized using a method involving four steps and described in ref 31. The sample solutions were prepared by gently stirring the surfactant in deionized water for 3 days. For equilibrium measurements, they were stored for at least 2 days at the desired temperature prior to measurements. Throughout the paper, the concentrations will be expressed in g cm^{-3}.

Static Light Scattering. For light scattering experiments, all solutions are filtered through a 0.22 μm Millipore (Sartorius) filter into the cylindrical scattering cells.

Static light scattering (SLS) and dynamic light scattering (DLS) experiments are performed on a standard setup[32] by means of a spectrometer equipped with an argon ion laser (Spectra Physics model 2020) operating at λ = 488 nm, an ALV-5000 correlator (ALV, Langen-Germany Instruments), a computer-controlled and stepping-motor-driven variable angle detection system, and a temperature-controlled sample cell. The temperature was 25 ± 0.1 °C unless otherwise noted. The scattering spectrum was measured through a band-pass filter (488 nm) and a pinhole (200 μm for the static experiments and 100 μm for the dynamic experiments) with a photomultiplier tube (ALV).

In the SLS experiments, the excess of scattered intensity $I(q)$ was measured with respect to the solvent, where the magnitude of the scattered wave vector q is given by

$$q = \frac{4\pi n}{\lambda} \sin\frac{\theta}{2} \tag{1}$$

In eq 1, n is the refractive index of the solvent (1.34 for water at 25 °C), λ is the wavelength of light in the vacuum, and θ is the scattering angle. In our experiments, the scattering angle θ was varied between 20° and 150°, which corresponds to scattering wave vectors q in the range from 6×10^{-3} to 3.2×10^{-2} nm^{-1}. The absolute scattering intensities $I(q)$, expressed in cm^{-1} (i.e, the excess Rayleigh ratios), were deduced by using a toluene sample reference for which the excess Rayleigh ratio is known.

Dynamic Light Scattering. In the dynamic light scattering experiments, the normalized time autocorrelation function $g^{(2)}(q, t)$ of the scattered intensity is measured.

$$g^{(2)}(q, t) = \frac{\langle I(q, 0)\, I(q, t)\rangle}{\langle I(q, 0)\rangle^2} \tag{2}$$

The latter can be expressed in terms of the field autocorrelation function or equivalently in terms of the autocorrelation function of the concentration fluctuations $g^{(1)}(q, t)$ through

$$g^{(2)}(q, t) = A + \beta|g^{(1)}(q, t)|^2 \tag{3}$$

where A is the baseline and β is the coherence factor which in our experiments is equal to 0.7−0.9. The normalized dynamical correlation function $g^{(1)}(q, t)$ of polymer concentration fluctuations is defined as

$$g^{(1)}(q, t) = \frac{\langle \delta c(q, 0)\, \delta c(q, t)\rangle}{\langle \delta c(q, 0)^2\rangle} \tag{4}$$

where $\delta c(q, t)$ and $\delta c(q, 0)$ represents fluctuations of polymer concentration at time t and zero, repectively.

(24) Barentin, C.; Liu, A. J. *Europhys. Lett.*, in press.
(25) Cates, M. E.; Candau, S. J. *Europhys. Lett.*, in press.
(26) Hoffmann, H.; Kalus, J.; Schwandner, B. *Ber. Bunsen-Ges. Phys. Chem.* **1987**, *91*, 99.
(27) Wang, K.; Karlsson, G.; Almgren, M.; Asakawa, T. *J. Phys. Chem. B* **1999**, *103*, 9237.
(28) Krafft, M. F.; Giulieri, F.; Riess, J. G. *Angew. Chem., Int. Ed. Engl.* **1993**, *32*, 741.
(29) Stähler, K.; Selb, J.; Candau, F. *Colloid Polym. Sci.* **1998**, *276*, 860.
(30) Hofmeister, F. *Arch. Exp. Pathol. Pharmakol.* **1888**, *24*, 247.
(31) Kotora, M.; Hájek, M.; Ameduri, B.; Boutevin, B. *J. Fluorine Chem.* **1994**, *68*, 49−56.
(32) Esquenet, C.; Buhler, E. *Macromolecules* **2001**, *34*, 5287−5294.

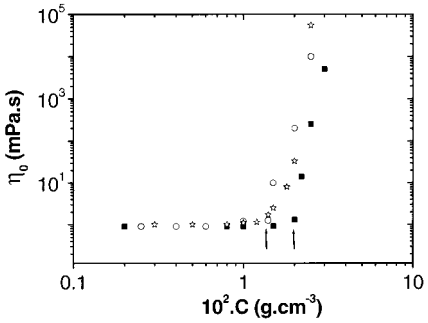

Figure 1. Zero-shear viscosity as a function of C_8F_{17} concentration in H_2O at 25 °C (○), at 30 °C (■), and in the presence of 20 mM NaF at 25 °C (☆). The arrows represent the crossover concentrations C_e between the two viscosity regimes for the salt-free systems.

Viscosimetry. The rheological measurements were performed with two different devices:

1. A Rheometrics RFS II fluid spectrometer using cone−plate geometry. The cell has a gap of 0.045 mm, an angle of 0.035 rad, and a diameter of 50 mm.

2. A Low Shear 30 viscometer using Couette geometry. The Couette cell has a gap of 0.5 mm and a height of 20 mm.

Both experiments were carried out with imposed strain equipment, and special care was taken to avoid water evaporation.

Experimental Results

In the Quiescent State. *Salt-Free Systems.* The cmc of the surfactant was determined by surface tension and conductimetry experiments. These two techniques provided slightly different values of the cmc: 1.3 mM (8×10^{-4} g cm^{-3}) by surface tension and 0.8 mM (5×10^{-4} g cm^{-3}) by conductimetry. These values are rather close to those reported for other fluorinated surfactants with different polar heads but with about the same length of the hydrophobic tail.[29]

The concentration dependences of the zero-shear viscosity at temperatures $T = 25$ °C and $T = 30$ °C are reported in Figure 1. The behavior is that reported for many salt-free micellar solutions. The viscosity is of the order of that of water from the cmc up to a concentration C_e that increases slightly with temperature, beyond which the viscosity rises sharply. The variation of the zero-shear viscosity with concentration for solutions containing a small amount of salt ($C_s = 20$ mM NaF) at $T = 25$ °C is also shown in Figure 1. The large increase of viscosity beyond C_e is generally attributed to the onset of entanglements between wormlike micelles. For regular polymers, C_e is significantly larger than the overlap concentration C^*.[33,34] As for the wormlike micelles, they are likely to entangle as soon as they overlap because of the very rapid micellar growth occurring above C^*[21] and we can assume that $C_e \approx C^*$.

It is generally admitted that a decrease of temperature or addition of salt increases the micellar size in the dilute regime, thus decreasing the crossover concentration. In Figure 1, whereas the temperature effect is that expected, the addition of salt does not change significantly the concentration C_e.

In the entangled regime, the viscoelastic properties are usually described by a polymer-like reptation model modified to take into account the micellar kinetics.[35−37] This model is well tested experimentally, at least for hydrocarbon surfactants.

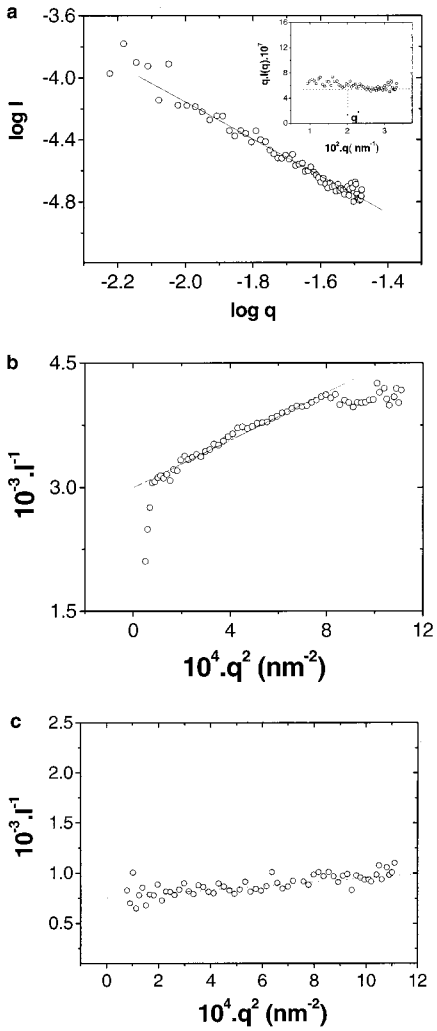

Figure 2. Scattering curves for different surfactant concentrations in H_2O. $I(q)$ represents the excess Rayleigh ratio expressed in cm^{-1}. (a) $C = 0.25 \times 10^{-2}$ g cm^{-3} ($C/C_e \sim 0.15$); (b) $C = 1.5 \times 10^{-2}$ g cm^{-3} ($C/C_e \sim 1$); (c) $C = 5 \times 10^{-2}$ g cm^{-3} ($C/C_e \sim 3.5$). The inset of (a) represents $q\,I(q)$ versus q.

Both static and dynamic light scattering experiments also reveal the existence of several concentration regimes. Figure 2 shows typical scattering curves in a log−log representation obtained at three different concentrations corresponding to $C/C_e \cong 0.15$, $C/C_e \sim 1$, and $C/C_e \sim 3.5$. At low concentration (Figure 2a), the data can be fitted with a straight line of slope −1.2 which is close to the slope of −1 characteristic of rodlike particles.[38] The representation $q\,I(q)$ as a function of q, given in the inset, shows that for wavevectors q larger than an ill-defined crossover wavevector $q^* \cong 2 \times 10^{-2}$ nm^{-1} one obtains indeed a q^{-1} variation of $I(q)$. There is no evidence of flattening of $I(q)$ in the low-q range, which would result from the finite size of the scattering entities. This suggests that particles with sizes larger than the experimental detection limit, that is, ≥200 nm, are present in the system. Depolarized light scattering experiments show that the depolarized component is negligible compared to the polarized one. This is evidence against the presence of very large anisotropic scatterers; we return to this point in the discussion.

(33) Graessley, W. W. *Polymer* **1980**, *21*, 258.
(34) Colby, R. H.; Rubinstein, M.; Daoud, M. *J. Phys. II France* **1994**, *4*, 1299.
(35) Cates, M. E. *J. Phys.* (*France*) **1988**, *49*, 1593.
(36) Cates, M. E. *Macromolecules* **1987**, *20*, 2289.
(37) Cates, M. E.; Candau, S. J. *J. Phys.: Condens. Matter* **1990**, *2*, 6869.
(38) See for example: Porod, G. In *Small-Angle X-ray Scattering*; Glatter, O., Kratky, O., Eds.; Academic Press: New York, 1982.

Table 1. Contin Analysis of DLS Results in Salt-Free Solutions of C_8F_{17} at $C = 0.25 \times 10^{-2}$ g cm^{-3} and $T = 25$ °C

	$10^3 \times q$ (nm^{-1})										
	8.86	11.71	14.47	17.12	19.64	22.01	24.21	26.23	28.05	29.66	31.04
$10^{-7} \times D_{fast}$ (nm^2/s)	6.64	7.58	7.97	7.22	8.26	7.71	7.68	7.75	7.62	9.26	8.22
$10^{-6} \times D_{slow}$ (nm^2/s)	**2.38**	**2.74**	**2.39**	**3.05**	**3.00**	**3.32**	**3.70**	**3.69**	**3.81**	**4.14**	**4.96**
A_{fast}/A_{tot}	0.066	0.102	0.088	0.126	0.140	0.146	0.160	0.166	0.180	0.192	0.204

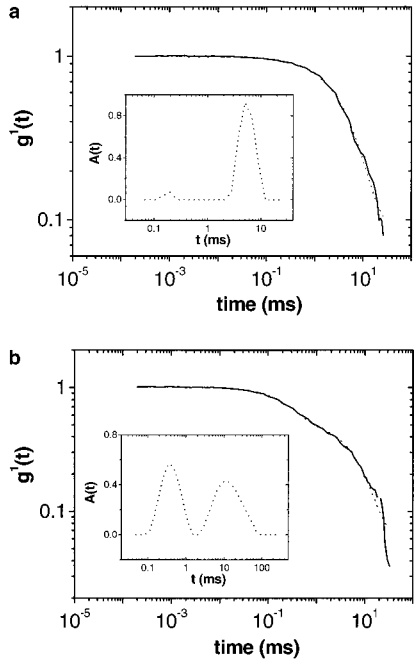

Figure 3. Dynamic light scattering in salt-free solution. Representation of $g^{(1)}(\tau)$ for $\theta = 30°$ for two concentrations. The dotted lines represents the Contin fits. (a) $C = 0.25 \times 10^{-2}$ g cm^{-3} ($C/C_e \sim 0.15$); (b) $C = 1.5 \times 10^{-2}$ g cm^{-3} ($C/C_e \sim 1$).

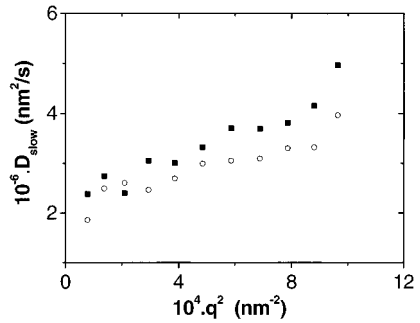

Figure 4. Variations of D_{slow} with q^2 at $C = 0.25 \times 10^{-2}$ g cm^{-3} without salt (■) and with 20 mM NaF (○).

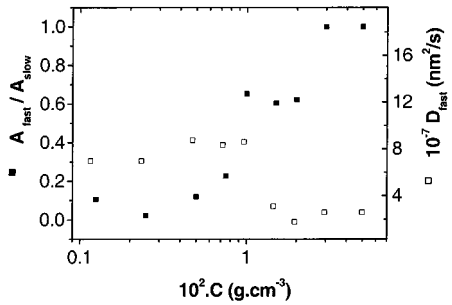

Figure 5. Variations of the relative amplitude A_{fast}/A_{tot} and the fast coefficient of diffusion D_{fast} as a function of surfactant concentration.

In the intermediate concentration range (Figure 2b), the scattering curves show some flattening, which is overcome in the low-q regime by an upturn revealing the presence of large particles. In the high-q range, $I(q)$ can be fitted with an Ornstein−Zernicke function $I(q) = I(0)/(1 + q^2\xi^2)$. In the representation $I(q)^{-1} = f(q^2)$ one obtains a linear part from which one extracts a correlation length $\xi \cong 22$ nm. The latter value must be considered as a rough estimate taking into account the non-negligible contribution of the scattering by large particles.

In the entangled systems, the scattering curves exhibit a slight decrease with q. In the $I(q)^{-1}$ versus q^2 representation (Figure 2c), one obtains a straight line whose slope gives $\xi = 16$ nm. Again, this value must be considered only as an estimate since such values are in the limit of the light scattering experimental window and would be more attainable by SANS experiments.

DLS experiments provide confirmatory evidence of the structural evolution of the system as the concentration is increased. In the concentration range extending from the cmc up to $\sim C_e$, the autocorrelation function of the scattered field $g^{(1)}(\tau)$ departs significantly from a single exponential, whereas beyond $\sim C_e$ it is close to a single exponential. The Laplace transform of $g^{(1)}(\tau)$ using the Contin procedure[39] gives two narrow modes with well-separated relaxation times (cf. Figure 3). At low concentration ($\sim 0.1 < C/C_e < \cong 0.3$), the contribution of the fast mode is only a small fraction of the total intensity and varies from ~20% at high q to less than 7% at low q (cf. Table 1). In fact, caution must be taken in asserting the bimodal shape of the autocorrelation function in that concentration range, considering the small amplitude of the fast mode revealed by the Laplace transform procedure. An equally good quality of fit can be obtained using a two-exponential function or a stretched exponential with an exponent γ varying from 0.7 at high q to 0.83 at low q.

Figure 4 shows the variation of D_{slow} with q^2. An extrapolation to zero q to obtain the translational diffusion coefficient of the particles and thus the hydrodynamic radius R_H through the Stokes−Einstein relation is not reliable as all the measurements are performed in the range $qR_G \gg 1$, where R_G is the average radius of gyration of the particles.

In the intermediate concentration range ($C/C_e \sim 1$), the field autocorrelation function becomes clearly bimodal with a predominance of the fast mode (cf. Figure 3b). This is in qualitative agreement with the scattering curve of Figure 2b showing the simultaneous presence of large particles and of a structure with a correlation length in the range of 20 nm. In that range, D_{fast} is independent of q whereas one still observes an increase of D_{slow} with q.

In the entangled regime, $C/C_e \geq 2$, the slow mode vanishes and $g^{(1)}(\tau)$ can be fitted with a single exponential whose decay rate provides D_{fast}.

Figure 5 shows the variations with concentration of D_{fast} and of the relative amplitude A_{fast}/A_{tot} of the fast mode. Up to $\sim C_e$, the behavior of the fast mode is close to that previously reported for other salt-free systems which did not exhibit any slow mode.[18,26] In particular, there is a small minimum in the vicinity of C_e. The constant value obtained for D_{fast} at $C > C_e$ is about 1 order of magnitude smaller than in the previously investigated systems.[18]

(39) Provencher, S. W. *Comput. Phys. Commun.* **1982**, *27*, 229.

Table 2. Contin Analysis of DLS Results in C_8F_{17} Solutions in the Presence of 20 mM NaF at $C = 0.25 \times 10^{-2}$ g cm^{-3} and $T = 25$ °C

	$10^3 \times q$ (nm^{-1})										
	8.86	11.71	14.47	17.12	19.64	22.01	24.21	26.23	28.05	29.66	31.04
$10^{-7} \times D_{fast}$ (nm^2/s)	6.73	6.61	6.96	7.19	6.55	7.24	6.82	7.26	6.86	6.76	6.46
$10^{-6} \times D_{slow}$ (nm^2/s)	**1.86**	**2.49**	**2.60**	**2.46**	**2.69**	**2.99**	**3.05**	**3.09**	**3.30**	**3.32**	**3.96**
A_{fast}/A_{tot}	0.13	0.12	0.18	0.186	0.204	0.236	0.262	0.249	0.315	0.338	0.299

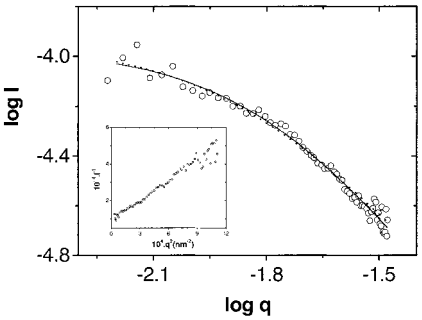

Figure 6. Scattering curves in a log−log representation for $C = 0.25 \times 10^{-2}$ g cm^{-3} with 20 mM NaF. The solid line represents the Fisher−Burford fit with $d = 2$. The dotted line represents the Fisher−Burford fit with $d = 5/3$. The inset represents $I(q)^{-1}$ versus q^2.

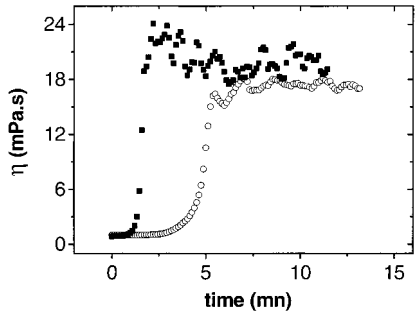

Figure 7. Viscosity as a function of time for a concentration $C = 0.8 \times 10^{-2}$ g cm^{-3} ($C/C_e \sim 0.5$) at two different shear rates: (○) 20 s^{-1} and (■) 50 s^{-1} at 30 °C.

Systems in the Presence of Salt. We have performed light scattering experiments on surfactant solutions with concentration $C = 0.25 \times 10^{-2}$ g cm^{-3} containing little enough salt ($C_s \sim 30$ mM) that one still observes the anomalous rheological features discussed in the next paragraph. Figure 6 shows the scattering curve obtained for a sample at a concentration of 0.25×10^{-2} g cm^{-3} containing 20 mM NaF. The comparison between this scattering curve and that corresponding to the salt-free solution at the same concentration (Figure 2a) reveals an important structural change. In presence of salt, one observes clearly a crossover from a Guinier behavior in the low-q range to an intermediate regime characterized by a power law. As most of the data lie in the crossover regime between the Guinier and the intermediate regime, one can use the Fisher−Burford expression[40] that has been applied to studies on fractal colloidal aggregates[41] and on wormlike micelles:[42]

$$I(q) = I(0)\frac{1}{1 + \frac{2}{3d}q^2{R_G}^2} \quad (5)$$

where d represents the exponent of the power law in the intermediate regime. Fits of the above expression to the scattering curves are shown in Figure 6, imposing for d the values of −2 characteristic of unperturbed chains and −5/3 corresponding to the excluded volume conformation.[43]

The fits provide a value of the radius of gyration in good agreement with the initial slope of the curve $I^{-1} = f(q^2)$ shown in the inset according to

$$I^{-1} = I(0)^{-1}\left(1 + \frac{q^2{R_G}^2}{3} + ...\right) \quad (6)$$

$R_G = 110 \pm 10$ nm from the Fisher−Burford fits, and $R_G = 103$ nm from the initial slope of $I^{-1}(q)$. The largest value of qR_G attainable in our experiments being ∼4, the qR_G range is too up-limited to get with accuracy the asymptotic exponent. Very similar results were obtained for solutions with $C_s = 30$ mM. As for the solutions with 5 and 10 mM NaF, the scattering curves decay monotonically without showing well-defined regimes. The correlation function of the scattered field can also be fitted by a two-exponential decay. The results of the fits are given in Table 2. From the extrapolation of D_{slow} to zero q, one obtains $R_H \sim 110$ nm, that is, a value close to that of R_G (cf. Figure 4).

Rheological Properties. The C_8F_{17} solutions show shear thickening and rheopectic behaviors in the concentration range cmc ≤ C ≤ C_e. The shear thickening occurs around a threshold of shear rate $\dot{\gamma}_c$ which depends on the temperature, the nature of the surfactant, and the salt concentration, as well as on C.

An illustration of this effect is given in Figure 7 that shows the time responses to steady shear flow for solutions at $C/C_e \cong 0.5$, $T = 30$ °C, and two different shear rates. One observes the typical behavior reported previously for other salt-free systems, characterized by an abrupt jump of the viscosity following a latency time T_R that decreases upon increasing the shear rate. At long times, the viscosity levels off to give a plateau showing erratic (perhaps chaotic) time dependence or in some cases oscillations.[44] Comparative experiments performed with a cone−plate cell with a gap of 0.045 mm or a Couette cell with a gap of 0.5 mm revealed that the shear rate $\dot{\gamma}_c$ is independent of the cell geometry (or gap). On the other hand, the latency time increases strongly with the gap size. As an example, for a solution at $C/C_e \cong 0.5$ and $T = 30$ °C, T_R was found to be ∼150 s with the 0.5 mm Couette cell and ∼25 s with the 0.045 mm cone−plate cell.

Figure 8 shows the effect of salt on the time responses for a solution at $C/C_e \cong 0.5$ and $T = 25$ °C. The critical shear rate increases with salt concentration. As an example, in the presence of 20 mM NaF, it is necessary to apply a shear rate of 80 s^{-1} to produce a shear thickening, whereas it is obtained with $\dot{\gamma} = 20$ s^{-1} for the solution containing 5 or 10 mM NaF. Also, the amplitude of the effect decreases upon increasing the salt content. These observations are in agreement with previous findings from flow birefringence experiments on TTAS.[5]

(40) Fisher, M.; Burford, R. *Phys. Rev. B* **1974**, *10*, 2818.
(41) Dietler, G.; Aubert, C.; Cannell, S. D.; Wiltzius, P. *Phys. Rev. Lett.* **1986**, *57*, 3117.
(42) Appell, J.; Porte, G. *Europhys. Lett.* **1990**, *12*, 185.
(43) De Gennes, P. G. *Scaling concepts in polymer physics*; Cornell University Press: Ithaca, NY, 1979.
(44) Bandyopadhyay, R.; Sood, A. K. Preprint, cond-mat/0012489.

Table 3. (A) Variation of $\dot{\gamma}_c^{-1}$ (s^{-1}) with Surfactant Concentration in Salt-Free Solutions at $T = 25$ °C. (B) Variation of $\dot{\gamma}_c^{-1}$ (s^{-1}) with Salt Concentration at $T = 25$ °C

(A) Variation of $\dot{\gamma}_c^{-1}$ (s^{-1}) with Surfactant Concentration in Salt-Free Solutions

	$10^2 \times C$ (g cm^{-3})						
	1.4	1	0.8	0.6	0.4	0.2	0.1
$\dot{\gamma}_c$ (s^{-1})	3 < .. < 5	5 < .. < 10	10 < .. < 20	∼20	∼30	∼30	∼40

(B) Variation of $\dot{\gamma}_c^{-1}$ (s^{-1}) with Salt Concentration

	NaF (mM)				
$10^2 \times C$ (g cm^{-3})	0	5	10	20	30
0.8	10 < .. < 20	∼20	20 < .. < 30	70 < .. < 80	90 < .. < 100
0.25	∼30	∼100[a]			

[a] $\eta_{max}/\eta_{min} \approx 2$.

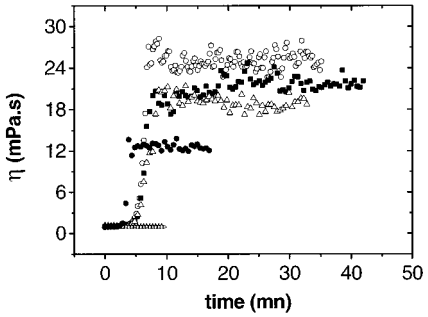

Figure 8. Viscosity as a function of time for solutions with surfactant concentration $C = 0.8 \times 10^{-2}$ g cm^{-3} ($C/C_e \sim 0.5$) at 25 °C: (○) without NaF at 20 s^{-1}, (■) 5 mM NaF at 20 s^{-1}, (△) 10 mM NaF at 20 s^{-1}, (☆) 20 mM NaF at 20 s^{-1}, (right-pointing triangle) 20 mM NaF at 40 s^{-1}, and (●) 20 mM NaF at 80 s^{-1}.

In Table 3 are given the variations of $\dot{\gamma}_c$ with both the salt content at given surfactant concentration and the surfactant concentration under salt-free conditions.

Slow Relaxations. Recent studies have reported the existence of slow relaxation processes following a shearing (at $\dot{\gamma} > \dot{\gamma}_c$) or a thermal pretreatment of the sample.[15] The results given below show that in C_8F_{17} solutions, a very slow time scale controls the disappearance of structural memory after the cessation of the shear or following a temperature change.

Figure 9 shows results obtained in a shear cycling experiment. First, the shear is applied on a sample at the equilibrium. Once the stationary viscosity is obtained (after 20 mn), the shear is stopped and then restarted 5 min later. For the two examples presented, the latency time is reduced by a factor of ∼2.

Figures 10 and 11 illustrate the effect of thermal cycling. A large increase of T_R is found in samples that have been held at a higher temperature for a long period beforehand (cf. Figures 10 and 11a). Interestingly, one observes the opposite behavior, that is, a decrease of the latency time, if one performs the opposite thermal cycling. The latency time is decreased by storing the sample for some time at a lower temperature (cf. Figure 11b).

The slow relaxation process can also be monitored by light scattering. Figure 12 shows the variations of scattered light as a function of time for a sample with $C/C_e \cong 0.5$ without salt and with 30 mM NaF after a sudden variation of temperature from 50 to 30 °C. In presence of salt, the structural relaxation takes place in less than 1 h, whereas in the salt-free system it is not completed after 7 h.

Discussion

Micellar Structure. A very unusual feature exhibited by the fluorinated C_8F_{17} surfactant in solution is the formation of very large micellar structures just above the cmc. The studies performed up to now either by light scattering or by SANS on hydrocarbon surfactants have concluded to the existence for $C < C_e$ of small rodlike micelles with a typical length of 40 nm.

However, one must quote a study performed by Lin et al.[45] on an equimolar mixture of allyl hexadecyldimethyl-

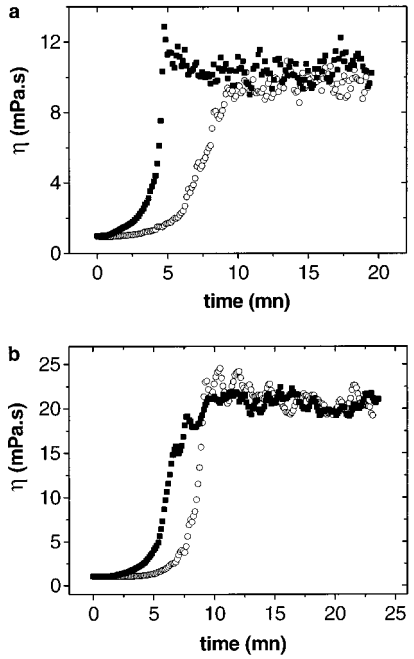

Figure 9. Effect of shear cycling for two solutions at 25 °C: (a) $C = 0.2 \times 10^{-2}$ g cm^{-3} ($C/C_e \sim 0.15$), shear rate = 30 s^{-1}; (b) $C = 0.8 \times 10^{-2}$ g cm^{-3} ($C/C_e \sim 0.5$), shear rate = 20 s^{-1}. (○) at equilibrium; (■) restarted after 5 min.

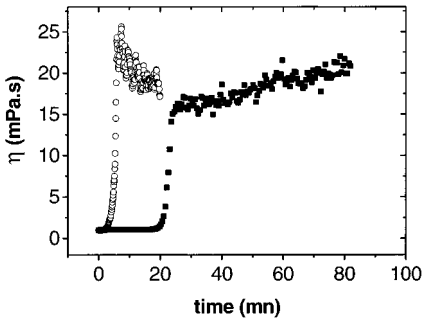

Figure 10. Effect of thermal cycling on a sample sheared at 25 °C. $C = 0.6 \times 10^{-2}$ g cm^{-3}; shear rate = 30 s^{-1}. (○) at equilibrium; (■) preheated at 50 °C.

(45) Lin, M. Y.; Hanley, H. J. M.; Sinha, S. K.; Straty, G. C.; Peiffer, D. G.; Kim, M. W. *Phys. Rev. E* **1996**, *53* (4), 302.

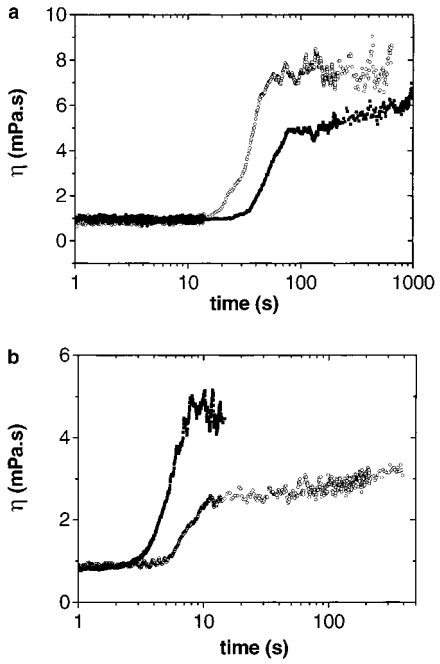

Figure 11. Effect of thermal cycling on the latency time on samples with $C = 0.8 \times 10^{-2}$ g cm^{-3}. (a) Shear rate = 50 s^{-1}: (○) stored at 30 °C; (■) stored for a few days at 50 °C and then for 30 min in the cell at 30 °C. (b) Shear rate = 300 s^{-1}: (○) stored at 40 °C; (■) stored for a few days at 30 °C and then for 30 min in the cell at 40 °C.

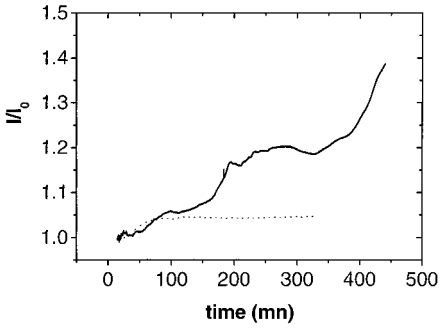

Figure 12. Variation of scattered light as a function of time for two solutions after a sudden variation of temperature from 50 to 30 °C, $\theta = 90°$, $C = 0.8 \times 10^{-2}$ g cm^{-3}: solid line, salt-free solution; dotted line, in the presence of 30 mM NaF.

ammonium bromide and sodium salicylate at $C/C_e = 0.62$. The scattering curves obtained in a large q range by light scattering and SANS could be fitted by a model of rigid rods with an exponential distribution of length and an average length of 230 nm. In that case, due to the salt NaBr formed from the mixture, the Debye−Hückel screening length was about 3 nm.

The fact that large micellar aggregates form just above the cmc indicates a very large end-cap energy, that should favor the formation of either very long linear micelles or, at least in theory,[35] a cascade of polydisperse rings. In the latter case, the minimum ring size would be controlled by the micellar persistence length.

In any case, the assessment of a structure for the surfactant self-assembly must take into account the following experimental observations:

(a) The results of Figure 2a suggest a rather rigid micellar conformation. An estimate of the persistence length l_p can be obtained from $q^* l_p = 1$ where q^* represents the scattering vector corresponding to the deviation from the horizontality of $q\,I(q)$ in the inset of Figure 2a. One finds $l_p \approx 50$ nm. According to the models of Odijk[46] and Skolnick and Fixman[47] derived for semiflexible polyelectrolytes under the assumption of a Debye−Huckel potential and in the limit where the Bjerrum length l_B is larger than the distance between two consecutive charges, the electrostatic persistence length l_e is given by

$$l_e = (4\kappa_s^2 l_B)^{-1} \tag{7}$$

Assuming a degree of ionization of 10% for the micellized surfactant and taking into account the ionic species resulting from the free surfactant (2 cmc), one finds $\kappa_s^{-1} \approx 10$ nm. Using the relation (7), one finds $l_e \approx 35$ nm. Assuming $l_p = l_e + l_0$, we obtain for the natural persistence length l_0 a value of ∼15 nm in agreement with previous findings.[48−50]

The addition of salt leads to an increased flexibility. The persistence length is likely reduced to the natural one. The effect of this on the scattering curve is outside of the q range probed by light scattering.

(b) At the concentration C_e, there is a relatively sudden drop in the characteristic length measured by both static and dynamic light scattering, from ≥200 to ∼20 nm. This suggests that in the dilute range there is a hidden length of ∼20 nm that does not show up in the experiments. This observation allows one to discard the hypothesis of a single population of linear micelles with sizes larger than 200 nm. In fact, in the range of concentration investigated such micelles would already be in the semidilute regime, considering the results obtained in other systems in the presence of an excess of salt (cetylpyridinium chlorate, $CPClO_3$).[51,52] In that case, one should observe a progressive decrease of both static and hydrodynamic correlation lengths upon increasing surfactant concentration.

Furthermore, for linear micelles with sizes of ≥200 nm, DLS should probe internal modes in the whole q range as observed for the $CPClO_3$ micelles. For a flexible chain, the characteristic decay time of the intermediate scattering function was predicted to vary like[43,53−56]

$$\tau^{-1} = A\frac{k_B T}{\eta_s} q^3 \tag{8}$$

where η_s is the viscosity of the solvent, τ^{-1} is the inverse first cumulant of the field autocorrelation function, and A is a numerical constant that depends on the quality of the diluent.

Figure 13 shows the dependence of the quantity $(\eta_s/qk_BT)D_{slow} \sim \eta_s\tau^{-1}q^{-3}$. The data tend to a plateau but only for q values larger than 1.5×10^{-2} nm^{-1}. One observes a similar behavior in the presence of salt.

(c) The surfactant aggregates are highly polydisperse in size. This is inferred from the observation that in salt-free dilute solutions, one does not observe any flattening of the $I(q)$ curves at low q. Also, the large increase of D_{slow} with q might indicate a large polydispersity even though

(46) Odijk, T. *J. Polym. Sci., Polym. Phys.* **1977**, *15*, 477.
(47) Skolnick, J.; Fixman, M. *Macromolecules* **1977**, *10*, 944.
(48) Porte, G.; Appell, J.; Poggi, Y. *J. Phys. Chem.* **1980**, *84*, 3105.
(49) Porte, G.; Poggi, Y.; Appell, J.; Maret, G. *J. Phys. Chem.* **1984**, *88*, 5713.
(50) Appell, J.; Marignan, J. *J. Phys. II* **1991**, *1*, 1447.
(51) Appell, J.; Porte, G.; Khatory, A.; Kern, F.; Candau, S. J. *J. Phys. II* (*France*) **1992**, *2*, 1045.
(52) Khatory, A.; Kern, F.; Lequeux, F.; Appell, J.; Porte, G.; Morie, N.; Ott, A.; Urbach, W. *Langmuir* **1993**, *9*, 933.
(53) Benmouna, M.; Akcasu, A. Z. *Macromolecules* **1978**, *11*, 1187.
(54) Akcasu, A. Z.; Han, C. C. *Macromolecules* **1981**, *14*, 1080.
(55) Lee, A.; Baldwin, P. R.; Oono, Y. *Phys. Rev. A* **1984**, *30*, 968.
(56) Oono, Y. *J. Chem. Phys.* **1983**, *79*, 4629.

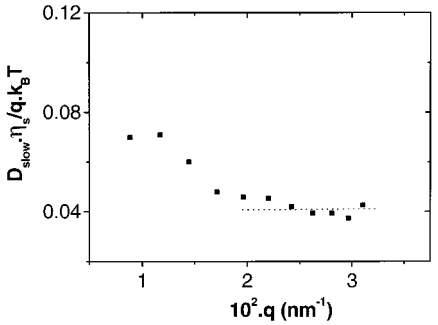

Figure 13. Variations of $(\eta_s/qk_BT)D_{slow}$ as a function of q at $C = 0.25 \times 10^{-2}$ g cm^{-3}.

this increase might arise in part from internal modes of the large aggregates. The addition of salt seems to decrease the polydispersity as the scattering curves can be fitted by an Ornstein−Zernicke function. Also, the variation of D_{slow} with q is less pronounced (cf. Figure 4).

(d) The autocorrelation function of concentration fluctuation is bimodal. This observation that might be questionable in salt-free systems at very low concentration becomes unambiguous close to C_e and also in the systems with 20 mM NaF. The most natural explanation is that the q-independent fast mode corresponds to collective fluctuations controlled by coupled micelle−counterion diffusion.[57,58] As for the slow mode, it could correspond to self-diffusion of the larger scattering entities present in the medium. This would be qualitatively similar to the situation encountered when approaching from below the sol−gel transition in polymer solutions. In that case, even though the transition involves mainly connectivity rather than concentration fluctuations, one observes indeed two modes. The slow relaxation time corresponding to the self-diffusion of the bigger aggregates diverges at the gel point.[59]

(e) The large entities revealed by light scattering are not highly anisotropic since no depolarized scattering is observed.

The above observation is evidence against the presence of compact bundles predicted by the model of Barentin and Liu,[24] as such bundles are expected to be anisotropic. Also, the effect of salt that induces a Gaussian conformation of the micelles would be difficult to explain in the framework of such a model.

One can envision various possible structures (schematized in Figure 14) to account for the light scattering results outlined above:

(i) The surfactant can self-assemble into semiflexible micelles with a very large (possibly bimodal) size polydispersity. The concentration C_e would correspond approximately to the overlap of the small micelles which are in the majority. This scheme disagrees with the model of Mackintosh et al.[21] that predicts a monodisperse distribution of small micelles. It is not compatible either with a large end-cap energy which would give a large free energy cost to such micelles. Note that the exponential polydispersity predicted for semiflexible micelles in the absence of Coulombic effects is probably not strong enough to explain the data.

(ii) Alternatively, the surfactant might form a cascade of micellar rings whose presence was predicted in early models of micellar growth and which has been reported

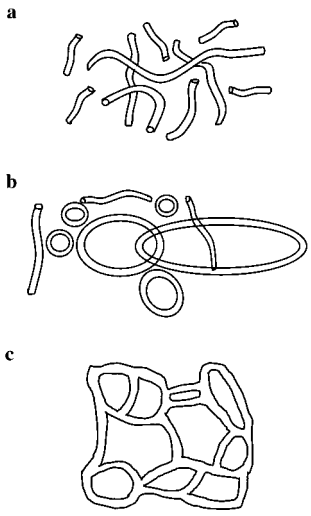

Figure 14. Schematic representation of possible structures of surfactant aggregates: (a) distribution of semiflexible linear micelles, (b) distribution of rings (possibly in equilibrium with linear micelles), and (c) microgels.

around the overlap threshold in a few other systems.[60,61] (The polydispersity is a power law times exponential which is much broader than the exponential alone.[35]) The larger rings would contribute mostly to the scattering at low q and would control the slow mode in DLS. In the absence of any open chains (as would apply at infinite end-cap energy), theory predicts a continuous polymerization transition in which the cascade of rings has an upper size limit which diverges at a critical concentration (beyond which there is a condensate of arbitrarily high molecular weight). This concentration is estimated from a threshold which we identify with C_e fixed by a (simultaneous) overlap criterion for rings of all sizes; around this threshold, one expects significant interlinking of the rings to form a topological network. The volume fraction involved is dominated by the contribution of smaller rings whose lower size limit is controlled by the persistence length l_p; in fact, C_e falls strongly as l_p is raised. In principle, critical fluctuation effects should be seen in the scattering data close to the critical point but these could be wiped out if the end-cap energy is not infinite (see below). Let us note that l_p decreases upon increasing concentration because of the screening due to the counterions that reduce the electrostatic component l_e. At C_e, the total persistence length is only slightly larger than the natural persistence length. The lower size limit of the rings should then be reduced because of an increased flexibility and should not be modified much by the addition of salt. This might explain why the values of C_e are almost the same with and without salt. The scenario does not easily explain the increase of C_e with temperature unless there is a stronger temperature dependence of l_p than suggested by theory.

(iii) A closely related suggestion is that the structure consists of an equilibrium involving both rings and open semiflexible micelles. This is the theoretical picture when the end-cap energy is not infinite; the ring-cascade survives, but the critical behavior is converted to a smooth crossover around C_e from mostly rings, via rings and open chains of similar size, to an entangled state in which the condensate is broken into finite fragments to form a conventional semidilute solution of open micelles. This

(57) Lin, S. C.; Lee, W.; Schurr, J. M. *Biopolymers* **1978**, *17*, 1041.
(58) Tivant, P.; Turq, P.; Drifford, M.; Magdelenant, H.; Menez, R. *Biopolymers* **1983**, *22*, 643.
(59) Munch, J. P.; Ankrim, M.; Hild, G.; Candau, S. J. *J. Phys., Lett.* **1983**, *44*, 73.
(60) In, M.; Aguerre-Chariol, O.; Zana, R. *J. Phys. Chem.* **1999**, *103*, 7747.
(61) Bernheim-Groswasser, A.; Zana, R.; Talmon, Y. *J. Phys. Chem. B* **2000**, *104*, 4005.

smoothed-out scenario is more in line with the experimental observations. Variation of C_e with temperature is more natural since there is a strong effect on the ring−chain equilibrium via the Boltzmann factor for ring opening. On the other hand, one might then expect a stronger salt effect than that observed (for the same reason).

(iv) From the results of light scattering, one could envision a fourth scenario in which the surfactant molecules self-assemble into polydisperse microgels made of interconnected micelles with an internal correlation length of the order of 20 nm (see Figure 4). The same factors which suppress end-caps will eventually stabilize intramicellar branching so that this scenario could be promoted by the distinctive packing considerations of fluorinated surfactants, mentioned in the Introduction. The concentration C_e would correspond to the overlap of the microgels, independent of the salt content (for the same reason as in the rings-only scenario outlined above). The fast diffusion mode could be due to the self-diffusion of the microgels. However, the microgel particles would have to be ragged (fractal) rather than compact in order to reconcile the fairly low C_e with the rather small internal correlation length. Note also that a theory of micellar network formation[62] points toward bulk separation to a gel phase (rather than formation of discrete microgel fragments) when branching becomes favorable, but this theory neglects the entropy of ragged network fragments and so is not definitive.

For the various aggregate structures considered above, one would expect that well beyond C_e the aggregates transform into entangled solutions of long open chains with a correlation length controlled by the smaller micellar rods or rings or by the internal correlation length of the microgels.

Dynamic Properties. Let us now consider to what extent the dynamical observations are consistent with the four scenarios outlined above.

A striking observation is the very large shear thickening observed in the solutions of this fluorocarbon surfactant. The viscosity increases by a factor as high as 50 at $T =$ 20 °C and at concentrations close to C_e, just above the critical shear rate. Also, the shear thickening can be observed at very low concentrations close to the cmc. These features are common to several fluorocarbon surfactants, both anionic[3] and cationic.[29] One is tempted to link this behavior to the presence of large aggregates in solution. Other experiments to be reported in a forthcoming paper show that both large nonlinear effects and large scattering entities are observed in solutions of a gemini surfactant for which one also expects a large end-cap energy.[63,64]

From a theoretical point of view, the model of ref 25, based on the existence of interlinked rings in the quiescent state characterized by a local delinking time τ_{link}, might account for several of the main experimental observations. (The interlinked rings are assumed to be close to, or above, the topological percolation transition; open chains are also present, so this represents the third scenario developed above.) Shear rates of the order $\dot{\gamma}_c \sim \tau_{link}^{-1}$ would disturb the kinetics of the system leading, in favorable cases, to an increased connectivity of the linked rings and a strong network alignment. The steady state would then comprise a mixture of rings and chains in various states of deformation, linkage, and alignment. According to this scheme, the critical shear rate $\dot{\gamma}_c$ controlled by the linking−delinking kinetics is a micellar characteristic. This is in agreement with the observation that $\dot{\gamma}_c$ does not depend on the geometry of the shear cell. On the other hand, the latency time that corresponds to the buildup of an aligned state is strongly dependent on the gap size. This kinetics approach of the critical shear rate can also put some light on the gradual suppression of the shear-thickening effect by adding salt. The birefringence results published earlier,[5] as well as the data presented in this paper and other data to be published,[63] show that $\dot{\gamma}_c$ increases with the salt content. If τ_{link} becomes very small in the presence of salt, then the interlinking of rings becomes effectively invisible.

Another challenging observation is the structural memory that persists for a very long time after a mechanical or thermal perturbation. This was explained in ref 25 by assuming that the perturbation induces a change in the ring/chain balance and the slow relaxation toward equilibrium is controlled by reversible scission kinetics. Reversible scission is not the only micellar reaction that could lead to delinking, but it is the only one that can alter the total number of chains present in the system. If it is much slower than stress relaxation, this will give structural memory that extends far beyond the time scales of flow response. For example, a thermal pretreatment at a much higher temperature will create more chains and leave fewer rings. This could explain the increased latency time. Also, the reverse behavior is expected in the case of a thermal pretreatment at a lower temperature, as observed indeed experimentally. The fact that the structural relaxation is faster in the presence of salt can be explained by a faster reversible scission kinetics as shown by T-Jump experiments.[63] Note that these effects, unlike those discussed in the previous paragraph, are critically dependent on the presence of open chains as well as rings in the quiescent state. Accordingly, they support the third scenario outlined above.

It is less clear to what extent the dynamical observations might also be reconciled with the fourth scenario (microgel fragments). Recall that a relaxation time of the order $1/\dot{\gamma}_c$ has to be present in the quiescent state; if this is the Zimm time of a gel particle, these must be fairly large. If they are, the kinetics of fusion and breakdown of the network gel fragments might be quite similar to that of a gel formed by topological interlinking of rings; it could be complicated further by the possible interlinking of the gel fractions and/or their conversion into rings or open chains under strong deformation. Two arguments against the microgel scenario from a dynamical point of view are as follows. (a) For conventional surfactants, there is evidence that cross-links between micelles slide freely and tend to decrease, rather than enhance, the viscosity[65] making it hard to explain the very high viscosity values for $C > C_e$ and in the shear-thickened state. (However, the mobility of the cross-links might be much lower in the case of fluoro-surfactants.) (b) Once significant cross-links are present, there is no longer a conserved quantity associated with the ring−chain equilibrium: the number of chains present varies with all types of micellar reaction, not just reversible scission. This undermines the explanation of structural memory put forward in ref 25.

Conclusion

The micellar structure of quiescent salt-free surfactant solutions is a key factor for understanding the shear-thickening mechanism and related effects.

(62) Drye, T. J.; Cates, M. E. *J. Chem. Phys.* **1992**, *96*, 1367.
(63) Oelschlaeger, C.; Waton, G.; Candau, S. J.; Cates, M. E. To be published.
(64) Weber, V. Unpublished results.
(65) Lequeux, F. *Europhys. Lett.* **1992**, *19* (8), 675.

The commonly accepted picture of rodlike micelles with an average length of a few dozens of nanometers[12,14,22,23] cannot account for the values of the critical shear rates obtained experimentally in the framework of the early models.[6,9,14] The determination of the average micellar length in SANS experiments is rendered complicated by the effect of the electrostatic interactions that leads to a peak in the static scattering curve and by the polydispersity of the scattering entities. The data are often analyzed by using a model combining the form factor of rigid cylinders and the structure factor given by the Hayter−Penfold approach.[66] In such a procedure, the position of the maximum in the scattering curves was found to be very sensitive to the average length of the rods, but the model of rigid cylinders was assumed a priori. A fit of the data using the form factor of a toroidal micelle rather than that of a linear cylinder would likely give an equally good agreement. Furthermore, the detection of the presence of very large particles in the systems requires an investigation of the low-q range, accessible only by light scattering. It is significant that the only study performed to our knowledge by combining SANS and light scattering (using the same procedure as above) concluded to the presence of very long rods (∼230 nm). Also, recent light scattering measurements in low ionic strength solutions of the 12-2-12 gemini surfactant showed unambiguously the presence of particles with sizes of ≥0.1 μm,[63,64] that were not detected in earlier SANS experiments.[17]

The DLS and SLS results reported in this paper show that the fluorocarbon surfactant investigated forms micellar aggregates with sizes of ≥100 nm in the concentration range cmc ≤ C ≤ C_e both under salt-free conditions and in the presence of small amounts of NaF (C_s ≤ 30 mM). If the quiescent state of the solution is different from what was assumed up to now, then new mechanisms for shear thickening can be envisioned. Still, we do not have any proof that the morphology of the micellar aggregates is the same for all systems showing shear thickening. As a matter of fact, previous light scattering studies on a single-chain hydrocarbon surfactant with a highly bound counterion did not give evidence of very large micellar aggregates,[18,26] but these systems show a weaker shear thickening (<4 close to C*, <2 at C*/2) and exhibit a higher critical shear rate ($\dot{\gamma}_c$ ≥ 100 s^{-1}) than the one studied here. Further light scattering experiments on other systems showing a large shear-thickening effect would be very useful to check a possible correlation between the nonlinear effects and the micellar structure in the quiescent state.

Referring back to the systems investigated here, the structure of the aggregates observed experimentally cannot be assessed unambiguously. However, the experimental observation that the correlation length drops sharply from ∼100 to ∼20 nm at C_e suggests the presence of either highly polydisperse linear or ring micelles or fractal aggregates (microgels) with an internal correlation length of ∼20 nm. The solutions with concentration C ≤ C_e exhibit a very large shear-thickening effect (up to 50) whose characteristics are strongly sensitive to either thermal or mechanical pretreatment of the samples. The dynamical observations appear to be consistent with the existence in the quiescent state of polydisperse interlinked micellar rings characterized by a local delinking time, as proposed in a recent model.[25] In this model, the reversible scission kinetics was assumed to control the slow relaxation processes following a thermal or mechanical perturbation. Light scattering experiments (not described here) performed in the semidilute regime at $C = 3 \times 10^{-2}$ g cm^{-3} show no detectable memory effect in a thermal cycling, whereas the zero-shear viscosity was found to evolve very slowly (over 1 day) toward its equilibrium value. At such a concentration, one expects that the surfactant forms very long entangled linear micelles. Both the scattered intensity and the cooperative diffusion coefficient are controlled by the correlation length of concentration fluctuations which is not expected to vary significantly with temperature. This would explain why these parameters do not exhibit any slow relaxation after perturbation of the system. In contrast, the rheological behavior depends strongly on the average length of the micelle whose equilibrium value is controlled by the reversible scission kinetics. The above observations provide further support to the assumption that the reversible scission process is a key factor for the slow structural relaxation.

As a final remark, the formation of very large micellar aggregates results from the combination of a packing parameter favoring the formation of cylindrical micelles and of a very large end-cap energy. These characteristics require a delicate balance between the degree of binding of the counterion and the hydrophobicity of the tails. Cationic fluorocarbon surfactants associated with the Cl^- counterion whose binding is much weaker than that of Br^- self-assemble into globular micelles.[27] Addition of small amounts of binding salt transforms them into wormlike micelles. At the opposite extreme, nonionic single-chain fluorocarbon surfactants associate at high dilution into vesicles.[28] The structure of the aggregates formed from fluorosurfactants appears to be very sensitive to the molecular parameters as compared with that of the analogous hydrocarbon surfactants.

Acknowledgment. We are indebted to O. Gavat who synthesized the fluorocarbon surfactant used in this study. We also thank E. Mendes for instructive discussions.

LA015687V

(66) Hayter, J. B.; Penfold, J. *Mol. Phys.* **1981**, *42*, 109−118.